EurJIC
European Journal of Inorganic Chemistry

Research Article
doi.org/10.1002/ejic.202400251

Chemistry Europe
European Chemical Societies Publishing

www.eurjic.org

Blue-Emissive Fluorescent Zinc(II) Complexes with Bis(imidazo[1,5-*a*]pyridine)methane Ligands

Gioele Colombo,[a] Anita Cinco,[a, b] Chiara Vola,[a] Bruno Therrien,[c] G. Attilio Ardizzoia,[a] and Stefano Brenna*[a]

Three bis(imidazo[1,5-*a*]pyridine)methane derivatives (bis(1-methylimidazo[1,5-*a*]pyridin-3-yl)methane, $\mathbf{L^H}$; 3,3′-(ethane-1,1-diyl)bis(1-methylimidazo[1,5-*a*]pyridine) $\mathbf{L^{Me}}$; 3,3′-(2-phenylethane-1,1-diyl)bis(1-methylimidazo[1,5-*a*]pyridine), $\mathbf{L^{Bz}}$) have been synthesized, and fully characterized in solution (^{1}H and ^{13}C NMR spectra) and in the solid state (X-ray). In particular, $\mathbf{L^H}$ has been prepared in high yield (75%) under very mild conditions (water, 60 °C), offering an alternative route to those reported in the literature. $\mathbf{L^{Me}}$ and $\mathbf{L^{Bz}}$ have been obtained from $\mathbf{L^H}$ by functionalization of the methylene bridge. The bis(imidazo[1,5-*a*]pyridine)methane compounds have been coordinated to a zinc(II) center, leading to tetrahedral complexes of general formula $[Zn(\mathbf{L^R})_2](ClO_4)_2$ (R = H, Me, Bz), which showed a bright fluorescent emission with (*x*,*y*) color coordinates very close to standard blue. TD-DFT have been employed to describe the Frontier Molecular Orbitals (FMOs) participating in electronic transitions, highlighting the main transition as $^1(\pi\text{-}\pi^*)$ transition in the bis(imidazo[1,5-*a*]pyridine)methane and a mixed intra-ligand (^{1}ILT) and ligand-to-ligand (^{1}LLT) transition in the complexes.

Introduction

Imidazo[1,5-*a*]pyridines represent a highly significant class of heterocyclic compounds, widely acknowledged in the literature for their notable photophysical and biological properties.[1] Their straightforward synthetic routes make them appealing building blocks for drug synthesis, particularly for antibacterial[2] and antitumoral[3] agents. In some instances, they act as apoptosis inducers and contribute to the treatment of Alzheimer's disease. Besides this, when properly functionalized, they find application as ligands in the synthesis of transition metal compounds,[4] often showcasing significant luminescent behavior.

Some bis(imidazo[1,5-*a*]pyridines) have been previously reported, either as dimeric species[5] or *trans*-ethylene-[6] or phenylene-bridged[7] derivatives. Conversely, very few papers can be found in the literature regarding bis(imidazo[1,5-*a*]pyridine)methane derivatives showing a methylene bridge between the two heterocyclic fragments. Döring[8] first reacted 1-methyl-3-[(1-methylimidazo-[1,5-*a*]pyridin-3-yl)methyl]imidazo[1,5-*a*]pyridine with $[(PPh_3)_2Ni(Mes)Br]$[9] (Mes = 2,4,6-trimethylphenyl) in the presence of sodium bis(trimethylsilyl) amide (Figure 1a). The resulting nickel(II) complex **I**, where the deprotonated bis(imidazo[1,5-*a*]pyridine)methane skeleton behaves as a β-diketiminate ligand, showed very interesting catalytic activity in the dimerization of propylene when activated with $Et_2AlCl{\cdot}EtAlCl_2$. Later, Lahiri[10] and coworkers first demonstrated the non-innocent redox behavior of these ligands in the reaction with a ruthenium(II) center under basic, anaerobic conditions (Figure 1b, **II** and **III**). More recently, he observed a similar non-innocent behavior when a methyl group was introduced on the methylene bridge (Figure 2, **IV**), whereas in the reaction towards metal acetates $(M(OAc)_x$, $x = 1$, M = Ag; $x = 2$, M = Zn, Cu, Pd)[11] the nature of the final products strongly depended on the metal acetate used and the substitution on the ligand skeleton (Figure 2). Indeed, when a stoichiometric amount of $Pd(OAc)_2$ or AgOAc was used, an oxidative dimerization of the ligand to species **V** occurred, though treatment with catalytic $Pd(OAc)_2$

[a] G. Colombo, A. Cinco, C. Vola, G. A. Ardizzoia, S. Brenna
Department of Science and High Technology, University of Insubria and CIRCC, Via Valleggio 9, 22100 Como, Italy
E-mail: stefano.brenna@uninsubria.it

[b] A. Cinco
Department of Science, Technology and Society, University School for Advanced Studies IUSS, Palazzo del Broletto, Piazza Vittoria 15, 27100 Pavia, Italy

[c] B. Therrien
Institute of Chemistry, Université de Neuchâtel, Avenue de Bellevaux 51, CH-2000 Neuchâtel, Switzerland

Supporting information for this article is available on the WWW under https://doi.org/10.1002/ejic.202400251

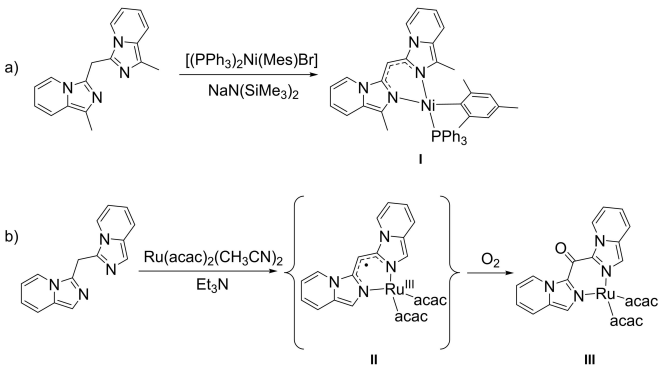

Figure 1. Nickel and ruthenium complexes with bis(imidazo[1,5-*a*]pyridine)methane ligands reported by (a) Döring (ref.[8]) and (b) Lahiri (ref.[10]).

Research Article
doi.org/10.1002/ejic.202400251

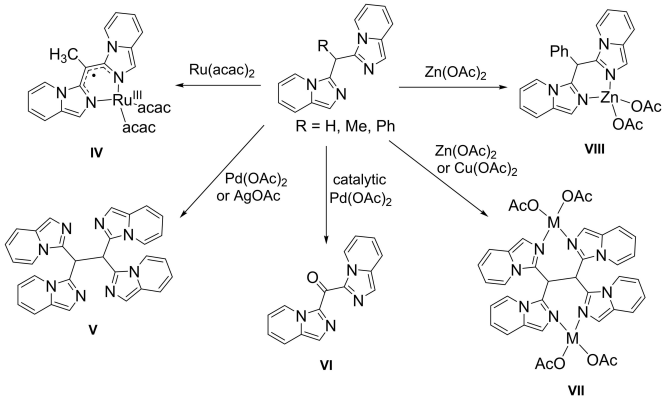

Figure 2. Reactivity of bis(imidazo[1,5-*a*]pyridine)methanes with metal acetates, reported by Lahiri (ref.[11]).

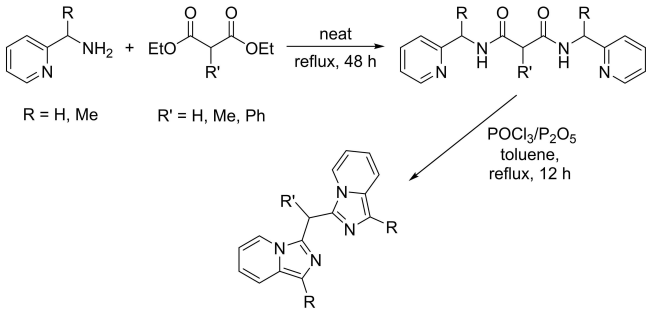

Scheme 1. Two-steps procedure commonly followed for the synthesis of bis(imidazo[1,5-*a*]pyridine)methane ligands.[8,10]

resulted in the oxidation to bis(imidazo[1,5-*a*]pyridin-3-yl)methanone **VI**. Oxidative dimerization was also observed in the reaction with $Zn(OAc)_2$ and $Cu(OAc)_2$, but in these cases dinuclear complexes (**VII**) were isolated instead of the free dimeric ligand. Finally, a mononuclear zinc(II) complex was isolated from $Zn(OAc)_2$ when the steric hindrance on the methylene bridge was increased by introducing a phenyl substituent (**VIII**).

In our ongoing investigation on the coordination chemistry of *N*-based multidentate ligands, we also deeply explored differently substituted *N*,*N*- and *N*,*O*-bidentate imidazo[1,5-*a*]pyridines[12] as potential ligands especially towards zinc(II),[12] silver(I)[12] and boron(III)[13] centers. Recently, we have focused our attention on the less explored bis(imidazo[1,5-*a*]pyridine)methane ligands and in particular on their mononuclear zinc(II) complexes. Herein, we report the synthesis and characterization of these zinc(II) derivatives, together with their attractive blue, fluorescent emission properties.

Results and Discussion

Synthesis of Ligands and Complexes

The synthesis of the previously reported bis(imidazo[1,5-*a*]pyridine)methane derivatives relies on a two-steps procedure (Scheme 1): condensation between diethyl malonate and 2-picolylamine first yields the corresponding bis-amide, which then undergoes cyclization under Bischler-Napieralski conditions.[8,10] Different substituents are introduced by starting from the substituted 2-picolylamine and/or diethylmalonate, with the compounds usually isolated as light-yellow powder in ca. 70% yield. With the aim of avoiding the use of the highly toxic phosphorous oxychloride, we searched for a possible alternative synthetic pathway. Following a well-established procedure,[13b] we have prepared (mono) imidazo[1,5-*a*]pyridines with aromatic substituents in position 3 of the heterocycle by reacting a 1-(pyridin-2-yl) ketone (2-acetylpyridine, benzoylpyridine, di-2-pyridyl ketone) with an aromatic aldehyde, in the presence of excess ammonium acetate, in acetic acid as solvent.

Optimizing this route, we have replaced the aromatic aldehyde with aqueous formaldehyde and avoided the use of acetic acid, performing the reaction in water at 60 °C. Starting from 2-acetylpyridine, under such very mild conditions, we obtained $\mathbf{L^H}$ in one step (Scheme 2a), with a yield comparable to the Bischler-Napieralski route. Then, an alkyl or benzyl substituent could be easily introduced on the methylene bridge of $\mathbf{L^H}$ by deprotonation with butyllithium followed by reaction with the corresponding alkyl or benzyl halide. This led to $\mathbf{L^{Me}}$ and $\mathbf{L^{Bz}}$ in 55% and 45% yields, respectively (Scheme 2b).

The zinc(II) complexes were prepared by reaction of zinc(II) perchlorate hexahydrate (1 eq.) with two equivalents of $\mathbf{L^R}$, in acetonitrile, at room temperature. The resulting complexes were formulated as $[Zn(\mathbf{L^R})_2](ClO_4)_2$ (Scheme 2c). The infrared spectra (Figures S1–S6) evidenced a slight shift (ca. 10 cm^{-1}) of

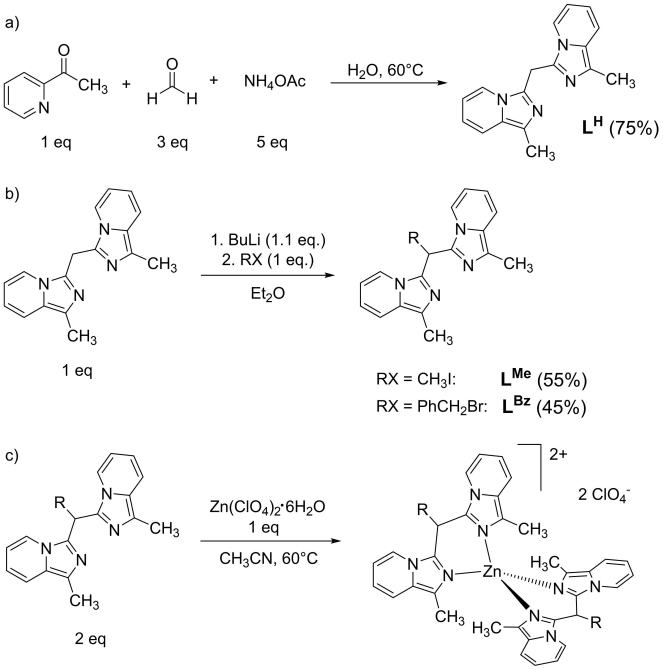

Scheme 2. a) Alternative synthetic conditions to obtain bis(imidazo[1,5-*a*]pyridine)methane $\mathbf{L^H}$ under mild conditions. b) Functionalization of $\mathbf{L^H}$ to give $\mathbf{L^{Me}}$ and $\mathbf{L^{Bz}}$. c) Synthesis of zinc(II) complexes.

Research Article
doi.org/10.1002/ejic.202400251

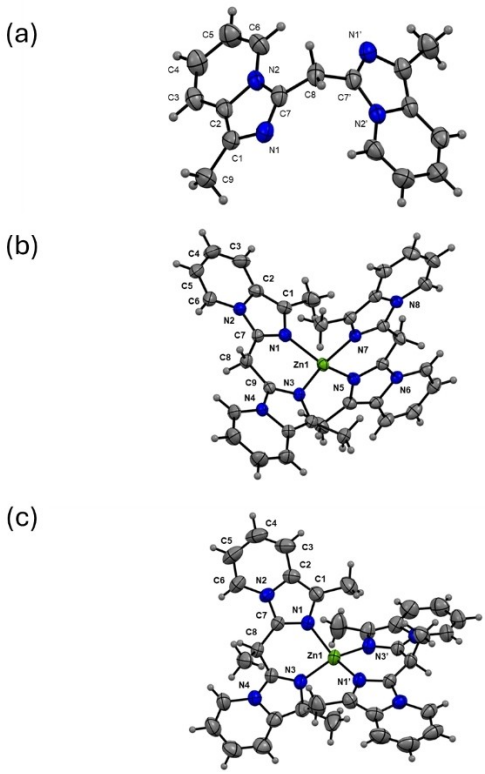

Figure 3. ORTEP representations (50% probability level ellipsoids) of (a) $\mathbf{L^H}$, (b) $[Zn(\mathbf{L^H})_2]^{2+}$ and (c) $[Zn(\mathbf{L^{Me}})_2]^{2+}$ (perchlorate anions omitted for clarity).

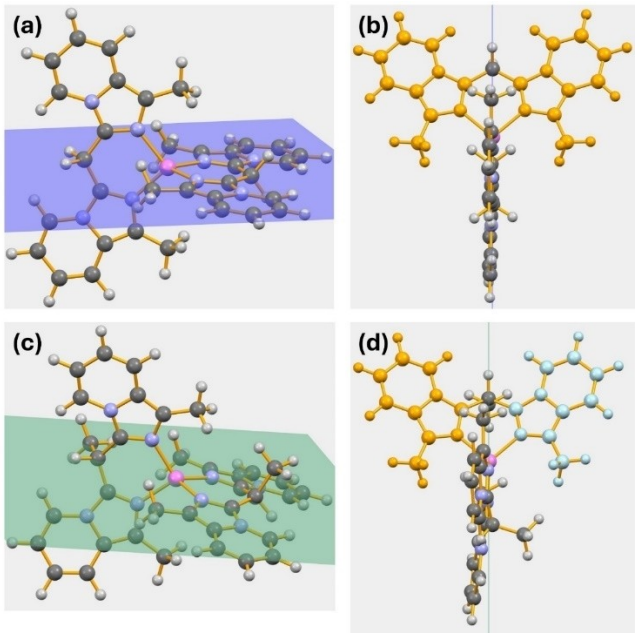

Figure 4. Different arrangements of bis(imidazo[1,5-*a*]pyridine)methane ligands in $[Zn(\mathbf{L^H})_2]^{2+}$ and $[Zn(\mathbf{L^{Me}})_2]^{2+}$: (a) The two imidazo[1,5-*a*]pyridine scaffolds placed in the plane comprising the zinc center, the two CH_2 groups and two N atoms (in position 2) of one ligand in $[Zn(\mathbf{L^H})_2]^{2+}$; (b) View along the plane in $[Zn(\mathbf{L^H})_2]^{2+}$, showing the highly symmetrical disposition of one ligand; (c) The two imidazo[1,5-*a*]pyridine scaffolds placed below the plane comprising the zinc center, the two CH_2 groups and two N atoms (in position 2) of one ligand in $[Zn(\mathbf{L^{Me}})_2]^{2+}$; (d) View along the plane in $[Zn(\mathbf{L^{Me}})_2]^{2+}$, showing the non-symmetrical disposition of one ligand. Perchlorate anions are omitted for clarity.

the sharp C=N stretching after coordination and the presence of uncoordinated perchlorate anions (broad band at 1070 cm^{-1}).

X-ray Characterization

Figure 3 shows the single-crystal X-ray structures of $\mathbf{L^H}$ and the complexes of $[Zn(\mathbf{L^H})_2](ClO_4)_2$ and $([Zn(\mathbf{L^{Me}})_2](ClO_4)_2$ salts (see Table S1 for crystallographic and structural refinement parameters). As expected, the N1 atoms are disposed in an anti-conformation in the free ligand $\mathbf{L^H}$, where the methylene bridge imposes an angle of 68.08° between the two imidazo[1,5-*a*]pyridine scaffolds (Figure S7). In both complexes, the zinc(II) center has a slightly distorted tetrahedral geometry (τ_4[14] being respectively 0.80 and 0.83 for $[Zn(\mathbf{L^H})_2]^{2+}$ and $[Zn(\mathbf{L^{Me}})_2]^{2+}$). The Zn···$OClO_3$ interactions measure 3.92(1) Å in $[Zn(\mathbf{L^H})_2](ClO_4)_2$ and 4.98(1) Å in $[Zn(\mathbf{L^{Me}})_2](ClO_4)_2$, thus excluding coordination of the perchlorate anions. In both $[Zn(\mathbf{L^R})_2]^{2+}$ complexes, bond lengths and angles are comparable (Table S2) to those reported in the literature for similar $[Zn(N{-}N)_2]^{2+}$ systems.[15]

Worthy of note, the bis(imidazo[1,5-*a*]pyridine)methane $\mathbf{L^H}$ has a different arrangement after complexation. Indeed, in $[Zn(\mathbf{L^H})_2](ClO_4)_2$ a plane comprising the zinc center, the two CH_2 groups and two N atoms (in position 2) of one ligand can be observed (Figure 4a); the two imidazo[1,5-*a*]pyridine cycles of one ligand lay in the plane, thus leading to a highly symmetrical arrangement, as highlighted by the view along that plane (Figure 4b, ligand in orange). On the contrary, the introduction of a substituent on the C7-C8-C9 bridge in $\mathbf{L^{Me}}$ forces the two bis(imidazo[1,5-*a*]pyridine)methane ligands in $[Zn(\mathbf{L^{Me}})_2]^{2+}$ to be in a non-planar configuration (with an angle of 17.16°): indeed, after considering the same plane as before (green plane in Figure 4c), the two imidazo[1,5-*a*]pyridine scaffolds on one ligand do not lay in the plane, but are slightly bent below. Concurrently, the methyl substituent on the methylene bridge points on one side of the plane (Figure 4d) thus making the two methyl groups on imidazo[1,5-*a*]pyridines non-equivalent, i.e. one on the same side of the substituent, the other on the opposite side (respectively, light blue and orange in Figure 4d). As a consequence, the two nitrogen atoms of one ligand coordinated to zinc have different environment, leading to a couple of enantiomers in the $[Zn(\mathbf{L^{Me}})_2]^{2+}$ complex (Figure S8).

The two enantiomers are better visualized by considering the concavity of the two bis(imidazo[1,5-*a*]pyridine)methane ligands originated after coordination, as sketched in Figure 5. Here, the two ligands in $[Zn(\mathbf{L^{Me}})_2]^{2+}$ are depicted in red and blue, respectively, whereas the zinc center is in green; hydrogen atoms and the methyl groups are omitted for clarity. If we arbitrarily place the red ligand ahead, its concavity points *down*, whereas the concavity of the blue moiety points *right*. As a result, if we report the concavity of the red ligand first, and blue ligand next, the enantiomer can be described as *down,right* (Figure 5a). By mirroring this compound, we obtain its enantiomer, defined as *down,left* (Figure 5b). Accordingly, the origin of the two enantiomers in $[Zn(\mathbf{L^{Me}})_2]^{2+}$ as a consequence of the concavity induced by the substituent on the methylene bridge,

Research Article
doi.org/10.1002/ejic.202400251

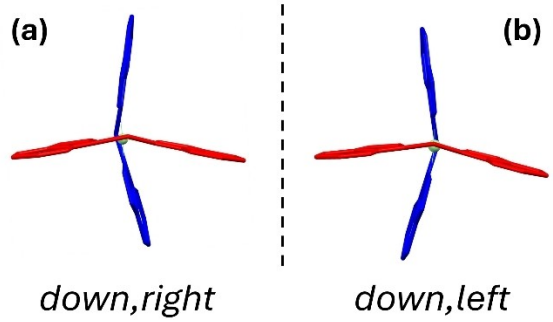

Figure 5. Inherent chirality in $[Zn(L^{Me})_2]^{2+}$ generated by ligand concavity. Red and blue sketches represent the two bis(imidazo[1,5-*a*]pyridine)methane ligands; zinc center in light green. The terms *down*, *right* and *left* indicate the concavity of the ligands. Arbitrarily, the concavity of the red ligand is reported first, followed by the concavity of the blue ligand. Thus, the two enantiomers can be described as *down,right* or *down,left*.

can be defined as a case of inherent chirality. Diversely, the flattening of the bis(imidazo[1,5-*a*]pyridine)methane ligands in the $[Zn(L^{H})_2]^{2+}$ cation does not allow to define a concavity for the ligand molecules, thus showing no inherent chirality. All these findings have been confirmed by NMR spectroscopy (*vide infra*).

NMR Investigation

In the ^{1}H NMR spectrum (CD_2Cl_2, 25 °C) of L^H (Figure S9), the signals associated to the imidazo[1,5-*a*]pyridine unit are clearly visible at 6.40–8.00 ppm (aromatic protons) and 2.43 ppm (CH_3 in position 1, CH_3-impy). The singlet at 4.70 is attributed to the methylene protons of the bridge. The corresponding resonances in ^{13}C NMR spectrum are respectively detected at 12.61 (CH_3-impy) and 27.12 ppm (CH_2) (Figure S10). Similarly, for L^{Me} and L^{Bz} the ^{1}H and ^{13}C NMR spectra show the expected signals of the aliphatic bridge (Figures S11 and S13): a quartet at 5.01 ppm (^3J = 7.4 Hz) and a doublet at 1.95 ppm (^3J = 7.9 Hz) for L^{Me}, and a triplet (5.11 ppm, ^3J = 7.9 Hz) and a doublet (3.85 ppm, ^3J = 7.9 Hz) for L^{Bz}. The related resonances in ^{13}C NMR spectra confirm the substitution pattern (Figures S12 and S14).

Overall, the coordination to the zinc center causes a slight shift of the resonances recorded in the ^{1}H NMR spectra: for $[Zn(L^H)_2](ClO_4)_2$, the singlet of the methylene protons was detected at 5.36 ppm (4.71 in free L^H), whereas the methyl in position 1 (CH_3-impy) of the imidazo[1,5-*a*]pyridine scaffold is upshifted from 2.44 (L^H) to 2.11 ppm ($[Zn(L^H)_2](ClO_4)_2$) (Figure S15). In ^{13}C NMR, both aliphatic resonances are upshifted to 11.74 ppm (CH_3-impy, 12.61 ppm in L^H) and 23.70 ppm (CH_2, 27.12 ppm in L^H), respectively (Figure S16). As discussed above, the introduction of the methyl group on the methylene bridge in L^{Me} led to a desymmetrization of the bis(imidazo[1,5-*a*]pyridine)methane ligands when coordinated to the zinc(II) center, as evidenced by the presence of two sets of signals attributable to CH_3-impy in the ^{1}H NMR (1.69 and 2.42 ppm) and ^{13}C NMR spectra (11.13 and 12.53 ppm), together with a small splitting of aromatic signals (Figures S17 and S18). A similar behavior was observed for $[Zn(L^{Bz})_2](ClO_4)_2$ (Figures S19 and S20). Consequently, due to the non-equivalence of CH_3-impy groups, $[Zn(L^{Me})_2]^{2+}$ is present as a pair of enantiomers (those previously indicated as *down,right* and *down,left*). To further prove this, the ^{1}H NMR spectrum of $[Zn(L^{Me})_2](ClO_4)_2$ was recorded in the presence of Δ-tris(tetrachloro-1,2-benzenediolato)phosphate(V)] tetrabutylammonium salt (Δ-TRISPHAT).[15] As expected, after addition of the chiral shift agent in a CD_2Cl_2 solution of $[Zn(L^{Me})_2](ClO_4)_2$, a pair of diastereoisomers was generated, as determined by the splitting of both signals attributed to CH_3-impy groups (Figure 6).

Fluorescence Properties

The photophysical data for all compounds are compiled in Table 1, while Figure 7 illustrates the normalized UV-vis and emission spectra recorded in dichloromethane solution ($5{\cdot}10^{-5}$ M) for ligands and complexes. The UV-vis traces of the ligands (Figure 7a) are characterized by two intense absorption peaks at around 240–280 nm and a low-energy absorption in the range 355–360 nm; these absorptions are thus not significantly influenced by the substituent on the methylene bridge. Such spectra closely resemble those of the corresponding complexes (Figure 7b), where a blue shift of both absorption (Δ = ca. 25 nm) and emission (Δ = ca. 30 nm) are observed compared to the free ligands. In particular, thank to this hypsochromic shift imposed by coordination, the zinc(II) derivatives all show a blue, fluorescent emission with (*x*,*y*) color coordinates very close to standard blue[16] (Figure S21). Blue emitters are still a major issue for luminescent materials development, since they are not as efficient as green or red counterparts.[17,18] Consequently, developing stable novel blue-emitting transition metal complexes that exhibit high color purity, quantum yield, and stability is a significant issue. All

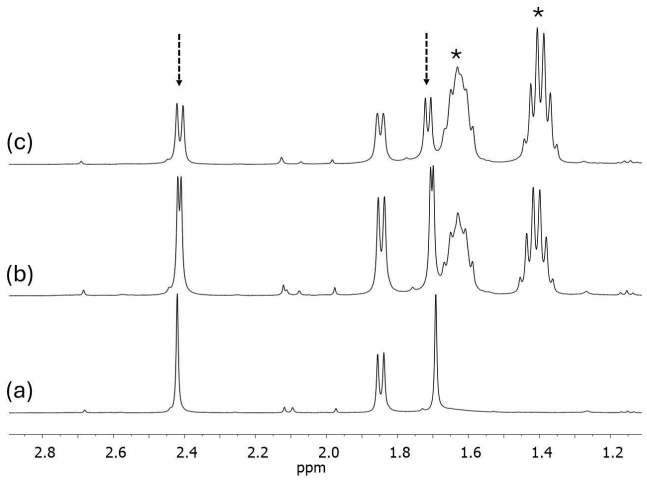

Figure 6. ^{1}H NMR spectra (CD_2Cl_2, 25 °C) of $[Zn(L^{Me})_2](ClO_4)_2$ in the absence (a) and presence of 1 equiv. (b) and 2 equiv. (c) of Δ-TRISPHAT. Resonances due to CH_3-impy groups are indicated by dashed arrows. Asterisks mark signals due to tetrabutylammonium.

Research Article
doi.org/10.1002/ejic.202400251

Table 1. Photophysical data for ligands L^R and complexes $[Zn(L^R)_2](ClO_4)_2$ in solution (CH_2Cl_2, $5\cdot10^{-5}$ M).

	ε (M^{-} cm^{-1})	λabs (nm)	λexc (nm)	λem (nm)	Stokes shift (eV)	ΦPL	τ (ns)
L^H	44062	356	356	450	0.73	0.84	19.7
L^{Me}	43749	355	357	452	0.75	0.66	16.0
L^{Bz}	33332	362, 377	355	447	0.65	0.69	12.2*
$[Zn(L^H)_2](ClO_4)_2$	10047	330	330	420	0.80	0.51	6.1
$[Zn(L^{Me})_2](ClO_4)_2$	12261	328	329	417	0.81	0.37	5.3
$[Zn(L^{Bz})_2](ClO_4)_2$	9802	328	335	418	0.81	0.31	6.1[a]

[a] Weighted average of a biexponential decay. L^{Bz}: $\tau_1 = 2.1$ (14.25 %), $\tau_2 = 13.9$ (85.75 %). $[Zn(L^{Bz})_2](ClO_4)_2$: $\tau_1 = 3.4$ (43.12 %), $\tau_2 = 8.1$ (56.88 %).

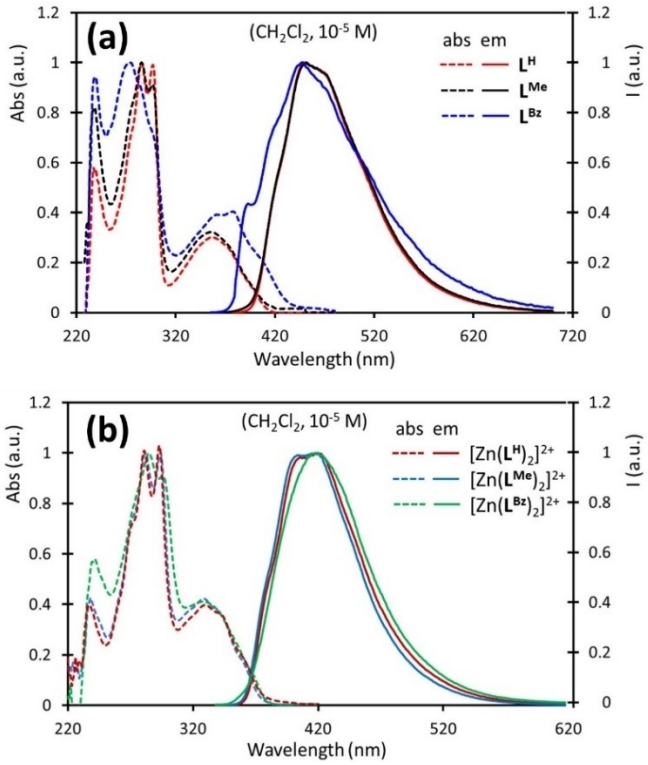

Figure 7. Normalized absorption (dashed lines) and emission (full lines) spectra of (a) ligands L^R and (b) complexes $[Zn(L^R)_2](ClO_4)_2$ recorded in solution (CH_2Cl_2, $5\cdot10^{-5}$ M).

species herein investigated exhibit a fluorescent behavior with a lifetime decay in the range of nanoseconds: ligands L^H and L^{Me} and complexes $[Zn(L^H)_2](ClO_4)_2$ and $[Zn(L^{Me})_2](ClO_4)_2$ display a mono-exponential fit of the decay curve, whereas decays of L^{Bz} and $[Zn(L^{Bz})_2](ClO_4)_2$ are described by a bi-exponential fitting. Reasonably, the higher mobility of the benzyl substituent increases possible interactions leading to non-radiative pathways. This is also corroborated by the shorter lifetime values recorded for L^{Bz} and $[Zn(L^{Bz})_2](ClO_4)_2$ compared to the other derivatives. Notably, lifetimes for ligands are longer (12.2–19.7 ns) than those of the corresponding complexes (2.1–6.1 ns). Absolute quantum yields are very good for all the compounds investigated, with a general decrease of PLQY upon coordination to zinc(II) and values up to 0.84 (for L^H) among ligands and 0.51 (for $[Zn(L^H)_2](ClO_4)_2$) among complexes (Table 1).

Computational Studies

Starting from the X-ray crystal structures of L^H, $[Zn(L^H)_2](ClO_4)_2$ and $[Zn(L^{Me})_2](ClO_4)_2$, the ground state (S_0) geometries of L^R ligands and of $[Zn(L^R)_2]^{2+}$ cations were optimized at the DFT/PBE0 level of theory. The fully optimized geometries of all compounds align well with the available X-ray data (refer to the Supporting Information for the coordinates of the optimized structures). The frontier molecular orbitals exhibit a strikingly similar configuration across all L^R derivatives (Figure 8): specifically, the HOMO and HOMO-1 are distributed over the whole two imidazo[1,5-*a*]pyridine moieties, with only a nearly negligible contribution from CH_2 observed in HOMO-1. The LUMO and LUMO + 1 orbitals are predominantly localized on the pyridine fragment of the ligands. In the $[Zn(L^R)_2]^{2+}$ cations, HOMO-1, HOMO, LUMO and LUMO + 1 orbitals are distributed over the two bis(imidazo[1,5-*a*]pyridine)methane molecules (Figure 9), with HOMO-1 and LUMO centered on one ligand, and HOMO and LUMO + 1 on the other. TD-DFT calculations allowed to define the main electronic transitions. Table 2 provides the energies of FMOs and the contributions of single orbital transitions related to the absorption at lower energy.

According to the shape of the FMOs, the main absorption in L^R derivatives can be described as a $^1(\pi\text{-}\pi^*)$ transition. In $[Zn(L^R)_2]^{2+}$ cations, the main transitions still involve frontier orbitals, with partial participation of higher (or lower) energy orbitals (Table S3). In these systems, besides the already mentioned $^1(\pi\text{-}\pi^*)$ intra-ligand transition (^{1}ILT) occurring within each ligand molecule, a ligand-to-ligand transition (^{1}LLT) from one bis(imidazo[1,5-*a*]pyridine)methane molecule to the other has to be considered.

Conclusions

In this paper, we reported an alternative synthesis of (bis(1-methylimidazo[1,5-*a*]pyridin-3-yl)methane, L^H, which was prepared under very mild conditions (water as solvent, 60 °C). This species could be easily functionalized on the methylene bridge by introduction of a methyl or benzyl substituent, leading to

Research Article
doi.org/10.1002/ejic.202400251

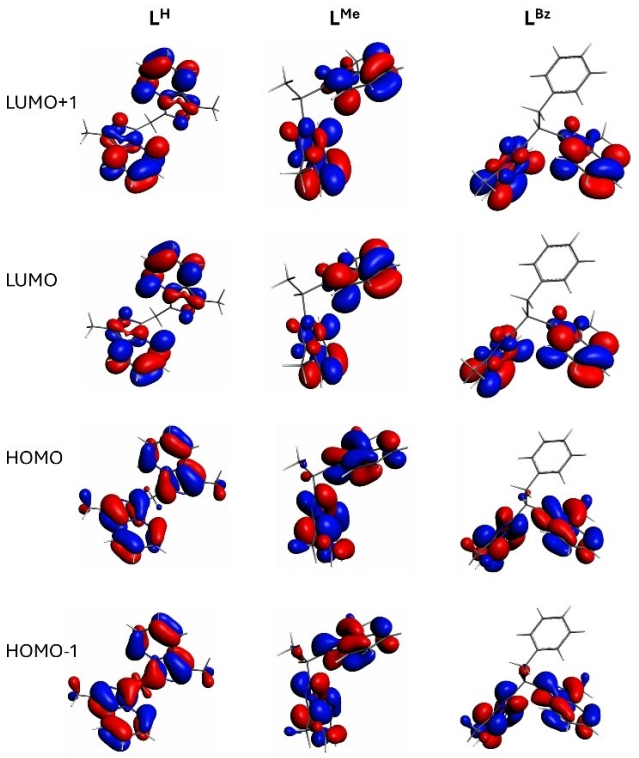

Figure 8. Frontier Molecular Orbitals (FMOs) calculated (DFT/PBE0) for ligands $\mathbf{L^R}$.

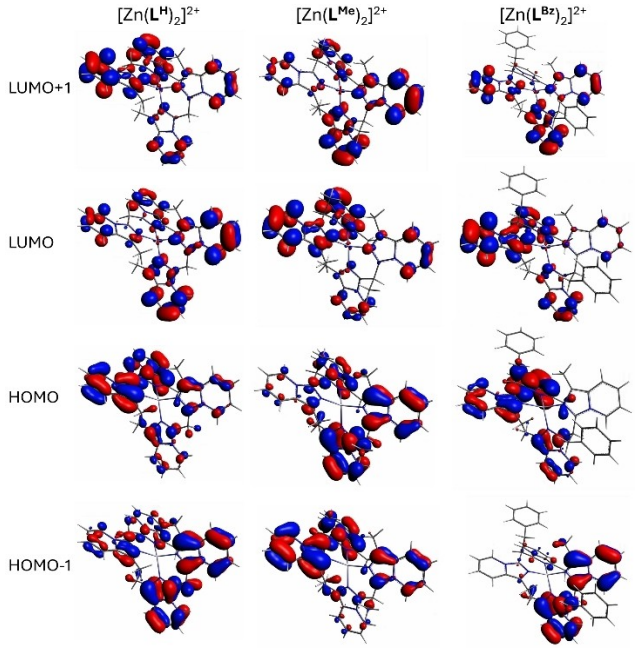

Figure 9. Frontier Molecular Orbitals (FMOs) calculated (DFT/PBE0) for cations $[Zn(\mathbf{L^R})_2]^{2+}$.

two new compounds indicated respectively as $\mathbf{L^{Me}}$ and $\mathbf{L^{Bz}}$. The corresponding zinc(II) complexes, $[Zn(\mathbf{L^R})_2](ClO_4)_2$ have been prepared and fully characterized. In particular, the introduction of the substituent in $[Zn(\mathbf{L^{Me}})_2](ClO_4)_2$ and $[Zn(\mathbf{L^{Bz}})_2](ClO_4)_2$ led to the generation of a couple of enantiomers, as also evidenced by NMR investigation. The photophysical properties of both ligands and complexes were investigated, and the zinc(II) complexes were characterized by a blue emission with color coordinates very close to standard blue. This work represents the first report to date on the fluorescence emission of these ligands and their complexes, thus paving the way to a new class of blue emissive complexes which could be employed for circularly polarized luminescence applications after resolution of the racemate mixture.

Experimental Section

General Information

Infrared Spectra (ATR) were acquired on a Thermo Scientific™ Nicolet™ iS20 FTIR Spectrometer with a 1 cm^{-1} resolution. Elemental analyses were obtained with a Perkin-Elmer CHN Analyzer 2400 Series II. NMR spectra were recorded with an AVANCE 400 Bruker spectrometer operating at 400 MHz for ^1H NMR and 100 MHz for $^{13}C\{^1H\}$ NMR. Chemical shifts are given as δ values in ppm relative to residual solvent peaks as the internal reference. *J* values are given in Hz. The UV-vis, excitation and emission spectra were measured using a fluorescence spectrometer (Edinburgh Instruments FS5) equipped with a 150 W continuous Xenon lamp as a light source and a detector for transmittance. All spectra were corrected for the wavelength response of the instrument; lifetime measurements were performed on the same FS5 Edinburgh Instruments equipped with an EPLED-320 (Edinburgh Instruments) as the pulsed source. Absolute fluorescence quantum yields in solution were determined using a PhotoMed GmbH K-Sphere Integrating Sphere (3.2 inch. diameter). Analysis of the lifetime decay curve and determination of absolute quantum yields were done using Fluoracle® Software package (Ver. 1.9.1) which runs the FS5 instrument. All chemicals have been purchased (TCI Chemicals, Fluorochem, Carlo Erba) and used without further purifications.

Synthesis of bis(1-methylimidazo[1,5-*a*]pyridin-3-yl)methane ($\mathbf{L^H}$)

A mixture of 6.87 g of ammonium acetate (89.1 mmol), 3.70 mL of a 40% m/m aqueous solution of formaldehyde (d = 1.09 g/mL, 53.5 mmol) and 2 mL of 2-acetylpyridine (d = 1.08 g/mL, 17.8 mmol) (ammonium:aldehyde:acetylpyridine = 5 : 3 : 1 molar ratio) was dissolved in 30 mL of deoxygenated water. The mixture was stirred at 60 °C for 24 hours under an inert atmosphere. The resulting suspension was diluted with 150 mL of water and extracted with CH_2Cl_2 (70 mL×3). The organic phase was dried over anhydrous Na_2SO_4, filtered and the solvent was removed under vacuum, yielding a yellow residue. It was suspended in 10 mL of acetone, the solid was filtered off and the mother liquor were dried under vacuum. The final product obtained is a light-yellow solid. Yield: 1.85 g (75%). Anal. Calcd (%) for $C_{17}H_{16}N_4$: C, 73.89; H, 5.84; N, 20.27. Found (%): C, 74.01; H, 5.97; N, 20.49. ^1H NMR (400 MHz, CD_2Cl_2, 298 K, *J* [Hz]): δ = 8.02 (d, *J* = 7.2 Hz, 2H), 7.28 (d, *J* = 9.1 Hz, 2H), 6.53 (dd, *J* = 9.0, 6.4 Hz, 2H), 6.42 (t, *J* = 6.5 Hz, 2H), 4.71 (s, 1H), 2.44 (s, 6H). ^{13}C NMR (100 MHz, CD_2Cl_2, 298 K): δ = 131.9, 127.8, 127.3, 121.9, 118.2, 116.9, 112.4, 27.3, 12.8.

Research Article
doi.org/10.1002/ejic.202400251

Table 2. Calculated energies of FMOs and percentage of main contributions of single orbital transitions.

Compound	HOMO-1[a]	HOMO[a]	LUMO[a]	LUMO + 1[a]	Percentage contributions	
L^{H}	−5.774	−5.595	−1.134	−1.078	HOMO→LUMO	78.2%
					HOMO-1→LUMO + 1	19.2%
L^{Me}	−5.786	−5.567	−1.118	−1.091	HOMO→LUMO + 1	62.4%
					HOMO→LUMO	16.3%
					HOMO-1→LUMO	13.0%
					HOMO-1→LUMO + 1	6.6%
L^{Bz}	−5.802	−5.567	−1.138	−1.092	HOMO→LUMO	81.8%
					HOMO-1→LUMO + 1	15.6%
$[Zn(L^{H})_2]^{2+}$	−6.677	−6.672	−2.095	−2.091	HOMO→LUMO	31.4%
					HOMO-1→LUMO + 1	28.6%
					HOMO→LUMO + 1	21.4%
$[Zn(L^{Me})_2]^{2+}$	−6.744	−6.730	−2.099	−2.095	HOMO→LUMO + 1	24.6%
					HOMO→LUMO	23.5%
					HOMO-1→LUMO + 1	21.4%
$[Zn(L^{Bz})_2]^{2+}$	−6.793	−6.783	−2.134	−2.131	HOMO-2→LUMO	45.3%
					HOMO-2→LUMO + 1	18.4%
					HOMO→LUMO	9.9%
					HOMO→LUMO + 1	6.1%

[a] Energies of FMOs are reported in eV.

Syntheses of 3,3′-(ethane-1,1-diyl)bis(1-methylimidazo[1,5-*a*]pyridine) (L^{Me}) and 3,3′-(2-phenylethane-1,1-diyl)bis(1-methylimidazo[1,5-a]pyridine) (L^{Bz})

A solution of butyllithium, prepared by dissolving 2.5 mL (1.6 M solution in hexanes) in diethylether (5 mL), was added dropwise at −78 °C to a suspension of 1.0 g of L^{H} (3.60 mmol) in 15 mL of diethylether. After addition, the mixture was stirred at room temperature for 2 h, then the halide (3.60 mmol) was slowly added. The resulting yellow suspension was stirred at room temperature for additional 12 h, then it was quenched with acidic (NH_4Cl) water (100 mL) and the organics extracted with methylene chloride (3×50 mL). After drying the organic phase over anhydrous Na_2SO_4 and filtering the salt off, the solvent was removed under vacuum. The residue was dissolved in diethyl ether (10 mL), the suspension filtered to remove unreacted L^{H} and the mother liquors concentrated under vacuum yielding a yellow-to-brown solid.

L^{Me}. Yield: 0.58 g (55%). Anal. Calcd (%) for $C_{18}H_{18}N_4$: C, 74.46; H, 6.25; N, 19.30. Found (%): C, 74.30; H, 6.18; N, 19.13. ^{1}H NMR (400 MHz, CD_2Cl_2, 298 K, *J* [Hz]): δ = 7.74 (d, *J* = 7.2 Hz, 2H), 7.28 (d, *J* = 9.1 Hz, 2H), 6.49 (dd, *J* = 9.1, 6.4 Hz, 2H), 6.31 (t, *J* = 6.7 Hz, 2H), 5.01 (q, *J* = 7.4 Hz, 1H), 2.46 (d, *J* = 12.0 Hz, 6H), 1.95 (t, *J* = 7.9 Hz, 3H). ^{13}C NMR (100 MHz, CD_2Cl_2, 298 K): δ = 136.0, 128.0, 127.1, 121.7, 118.4, 116.9, 112.4, 33.5, 15.8, 12.8.

L^{Bz}. Yield: 0.60 g (45%). Anal. Calcd (%) for $C_{24}H_{22}N_4$: C, 78.66; H, 6.05; N, 15.29. Found (%): C, 78.43; H, 5.84; N, 15.60. ^{1}H NMR (400 MHz, CD_2Cl_2, 298 K, *J* [Hz]): δ = 7.86 (d, *J* = 7.2 Hz, 2H), 7.26 (d, *J* = 9.2 Hz, 2H), 7.16–7.11 (m, 2H), 7.04 (d, *J* = 7.3 Hz, 2H), 6.49 (dd, *J* = 8.9, 6.5 Hz, 2H), 6.33 (t, *J* = 6.7 Hz, 2H), 5.11 (t, *J* = 7.9 Hz, 1H), 3.85 (d, *J* = 7.9 Hz, 2H), 2.44 (s, 6H). ^{13}C NMR (101 MHz, CD_2Cl_2, 298 K): δ = 139.9, 134.6, 129.6, 128.7, 128.0, 127.2, 126.9, 121.7, 118.4, 117.0, 112.5, 40.9, 12.8.

Syntheses of Zinc(II) Complexes

Zinc(II) perchlorate hexahydrate (0.32 g, 8.60 mmol) was added to a solution of ligand (17.2 mmol) in 15 mL of acetonitrile, and the mixture was stirred at 60 °C for 12 h. Then the solvent was removed under reduced pressure, and the residue was triturated with diethyl ether (15 mL). The yellow solid was filtered off, washed with diethyl ether and dried under vacuum.

$[Zn(L^{H})_2](ClO_4)_2$. Yield: 0.60 g (85%). Anal. Calcd (%) for $C_{34}H_{32}Cl_2N_8O_8Zn$: C, 49.99; H, 3.95; N, 13.72. Found (%): C, 50.18; H, 4.05; N, 14.02. ^{1}H NMR (400 MHz, CD_2Cl_2, 298 K, *J* [Hz]): δ = 8.74 (d, *J* = 7.2 Hz, 4H), 7.49 (d, *J* = 9.1 Hz, 4H), 7.10 (t, *J* = 6.6 Hz, 4H), 7.03 (t, *J* = 6.6 Hz, 4H), 5.35 (s, 4H), 2.11 (s, 12H). ^{13}C NMR (100 MHz, CD_2Cl_2, 298 K) δ 130.8, 128.7, 125.4, 123.0, 122.1, 118.2, 117.1, 23.9, 11.9.

$[Zn(L^{Me})_2](ClO_4)_2$. Yield: 0.48 g (66%). Anal. Calcd (%) for $C_{36}H_{36}Cl_2N_8O_8Zn$: C, 51.17; H, 4.29; N, 13.26. Found (%): C, 51.03; H, 4.35; N, 13.11. ^{1}H NMR (400 MHz, CD_2Cl_2, 298 K, *J* [Hz]): δ = 8.82 (dt, *J* = 23.0, 11.5 Hz, 4H), 7.55 (d, *J* = 9.1 Hz, 2H), 7.40 (t, *J* = 16.7 Hz, 2H), 7.16–6.95 (m, 8H), 6.09 (q, *J* = 7.0 Hz, 2H), 2.43 (s, 6H), 1.85 (d, *J* = 7.0 Hz, 6H), 1.7 (s, 6H).^{13}C NMR (100 MHz, CD_2Cl_2, 298 K): δ = 136.5, 135.9, 128.6, 125.6, 123.1, 123.0, 122.2, 122.0, 118.3, 117.4, 117.3, 29.2, 19.7, 12.8, 11.4.

$[Zn(L^{Bz})_2](ClO_4)_2$. Yield: 0.59 g (69%). Anal. Calcd (%) for $C_{48}H_{44}Cl_2N_8O_8Zn$: C, 57.81; H, 4.45; N, 11.24. Found (%): C, 57.58; H, 4.53; N, 11.04. ^{1}H NMR (400 MHz, CD_2Cl_2, 298 K, *J* [Hz]): δ = 8.34 (d, *J* = 7.3 Hz, 2H), 8.27 (d, *J* = 7.2 Hz, 2H), 7.42 (d, *J* = 9.2 Hz, 2H), 7.20 (d, *J* = 9.1 Hz, 2H), 7.12–7.03 (m, 6H), 6.90 (dd, *J* = 13.2, 6.6 Hz, 2H), 6.83–6.76 (m, 8H), 6.71 (t, *J* = 6.7 Hz, 2H), 6.12 (t, *J* = 7.8 Hz, 2H), 3.33 (d, *J* = 7.3 Hz, 4H), 2.56 (s, 6H), 1.39 (s, 6H). ^{13}C NMR (100 MHz, CD_2Cl_2, 298 K): δ = 135.5, 135.2, 134.6, 129.9, 129.6, 128.6, 128.5, 128.5, 126.4, 126.1, 122.9, 122.7, 122.2, 121.8, 117.9, 117.8, 116.8, 116.7, 44.0, 36.3, 13.5, 11.1.

Single-Crystal X-ray Structure Analyses

Crystals of $\mathbf{L^H}$, $[Zn(\mathbf{L^H})_2](ClO_4)_2$ and $[Zn(\mathbf{L^{Me}})_2](ClO_4)_2$ were mounted on a STOE STADIVARI Eulerian 4-circle diffractometer equipped with a Pilatus300 K detector, using Cu–Kα radiation (λ = 1.54186 Å). The structure was solved and refined by direct methods using the OLEX2 platform.[19] The H-atoms were included in calculated positions and treated as riding atoms, while the non-H atoms were refined anisotropically, using weighted full-matrix least-square on F^2. Crystallographic details are summarized in Table S1. Figures 3 and S7 were drawn with Mercury.[20] In $[Zn(\mathbf{L^{Me}})_2](ClO_4)_2$ a void of 68 Å^3 (≈20 electrons) was observed. This void was considered to be a highly disordered water molecule, and it was removed during refinement using the Mask algorithm from OLEX2.

CCDC-2348680 ($\mathbf{L^H}$), 2348681 ($[Zn(\mathbf{L^{He}})_2](ClO_4)_2$) and 2348682 ($[Zn(\mathbf{L^{Me}})_2](ClO_4)_2$) contain the supplementary crystallographic data for this paper. These data can be obtained free of charge via www.ccdc.cam.ac.uk/data request/cif, by e-mailing data request@ccdc.cam.ac.uk, or by contacting The Cambridge Crystallographic Data Centre, 12, Union Road, Cambridge CB2 1EZ, UK; fax: +44 1223 336033.

Computational Details

All calculations were carried out at the density functional (DFT) level of theory with the ADF2022.101 program package.[21] The PBE0 functional[22] was employed for all calculations. Frequency analyses were performed for all optimized structures to establish the nature of the stationary points. TD-DFT implemented in the ADF package was used to determine the excitation energies: the 30 lowest singlet-singlet excitations were calculated by using the optimized geometries. For geometry optimizations, C, N and O atoms were described through TZ2P basis sets [triple-ξ Slater-type orbitals (STOs) plus two polarization functions], Zn atoms were described through QZ4P basis sets [quadruple-ξ Slater-type orbitals (STOs) plus four polarization functions] and H atoms were described through TZP basis sets [triple-ξ Slater-type orbitals (STOs) plus one polarization function]. The corresponding augmented basis set was employed in TD-DFT calculations.[23] Restricted formalism, no-frozen-core approximation (all-electron) and no-symmetry constrains were used in all calculations. Solvent effects (CH_2Cl_2) were simulated employing the conductor-like continuum solvent model (COSMO)[24] as implemented in the ADF suite.

Author Contributions

Gioele Colombo: Methodology, Investigation, Data curation, Writing–Original Draft Preparation. Anita Cinco: Methodology, Investigation, Data curation, Writing–Original Draft Preparation. Chiara Vola: Methodology, Investigation, Data curation. Bruno Therrien: Methodology, Investigation, Data curation, Writing–Review and Editing. Stefano Brenna: Conceptualization, Methodology, Supervision, Funding Acquisition, Writing–Original Draft Preparation. G. Attilio Ardizzoia: Conceptualization, Software, Supervision, Funding Acquisition, Writing–Review and Editing.

Acknowledgements

This work was partially supported by University of Insubria (grant number DISAT2022-adrj002, G.C). This paper and related research have been partly conducted during and with the support of the Italian national inter-university PhD course in Sustainable Development and Climate change (link: www.phd-sdc.it) at the University School for Advanced Studies IUSS Pavia, Cycle XXXVIII, with the support of a scholarship financed by the Ministerial Decree no. 351 of 9th April 2022, based on the NRRP - funded by the European Union - NextGenerationEU - Mission 4 "Education and Research", Component 1 "Enhancement of the offer of educational services: from nurseries to universities" – Investment 4.1 "Extension of the number of research doctorates and innovative doctorates for public administration and cultural heritage" (A.C.). Open Access publishing facilitated by Università degli Studi dell'Insubria, as part of the Wiley - CRUI-CARE agreement.

Conflict of Interests

Authors declare no conflict of interests.

Data Availability Statement

The data that support the findings of this study are available from the corresponding author upon reasonable request.

Keywords: Blue emission · Zinc(II) · Fluorescence · DFT · N ligands

[1] a) G. Volpi, R. Rabezzana, *New J. Chem.* **2021**, *45*, 5737–5743; b) G. Volpi, *Asian J. Org. Chem.* **2022**, *11*, e202200171.
[2] Y. Q. Ge, F. R. Li, Y. J. Zhang, Y. S. Bi, X. Q. Cao, G. Y. Duan, J. W. Wang, Z. L. Liu, *Luminescence* **2014**, *29*, 293–300.
[3] a) A. Kamal, G. Ramakrishna, M. J. Ramaiah, A. Viswanath, A. V. Subba Rao, C. Bagul, D. Mukhopadyay, S. N. C. V. L. Pushpavalli, M. Pal-Bhadra, *Med. Chem. Commun.* **2013**, *4*, 697–703; b) K. Hoshi, M. Itaya, K. Tahara, A. Matsumoto, A. Tabata, H. Nagamune, Y. Yoshida, E. Hase, T. Minamikawa, T. Yasui, T. Katayama, A. Furube, K. Minagawa, Y. Imada, F. Yagishita, *RSC Adv* **2021**, *11*, 26403–26407.
[4] a) M. D. Weber, C. Garino, G. Volpi, E. Casamassa, M. Milanesio, C. Barolo, R. D. Costa, *Dalton Trans.* **2016**, *45*, 8984–8993; b) S. Pischedda, S. Stoccoro, A. Zucca, G. Sciortino, F. Ortu, G. J. Clarkson, *Dalton Trans.* **2021**, *50*, 4859–4873; c) Y.-W. Zhang, R. Das, Y. Li, Y.-Y. Wang, Y.-F. Han, *Chem. Eur. J.* **2019**, *25*, 5472–5479.
[5] F. Yagishita, K. Nomura, S. Shiono, C. Nii, T. Mino, M. Sakamoto, Y. Kawamura, *ChemistrySelect* **2016**, *15*, 4560–4563.
[6] G. L. Volpi, C. Garino, E. Priola, E. Artuso, P. Cerreia Vioglio, C. Barolo, A. Fin, A. Genre, C. Prandi, *Dyes Pigm.* **2018**, *157*, 298–304.
[7] G. Volpi, C. Garino, E. Conterosito, C. Barolo, R. Gobetto, G. Viscardi, *Dyes Pigm.* **2016**, *128*, 96–100.
[8] M. E. Bluhm, C. Folli, D. Pufky, M. Kröger, O. Walter, M. Döring, *Organometallics* **2005**, *24*, 4139–4152.
[9] A. Klein, *Z. Anorg. Allg. Chem.* **2001**, *627*, 645–650.
[10] S. Panda, S. K. Bera, P. Goel, A. K. Dutta, G. K. Lahiri, *Inorg. Chem.* **2019**, *58*, 11458–11469.
[11] S. Panda, R. Baliyan, S. Dhara, K.-W. Huang, G. K. Lahiri, *Dalton. Trans.* **2021**, *50*, 1664–16659.
[12] G. Colombo, G. A. Ardizzoia, S. Brenna, *Inorg. Chim. Acta* **2022**, *535*, 120849–120863.

[13] a) G. Colombo, A. Romeo, G. A. Ardizzoia, J. Furrer, B. Therrien, S. Brenna, *Dyes Pigm.* **2020**, *182*, 108636–108644; b) G. Colombo, G. A. Ardizzoia, J. Furrer, B. Therrien, S. Brenna, *Chem. Eur. J.* **2021**, *27*, 12380–12387; c) G. Colombo, A. Cinco, G. A. Ardizzoia, S. Brenna, *Colorants* **2023**, *2*, 179–193; d) G. Colombo, A. Cinco, J. Furrer, B. Therrien, S. Brenna, G. A. Ardizzoia, *Dyes Pigm.* **2023**, *220*, 111722.
[14] L. Yang, D. R. Powell, R. P. Houser, *Dalton Trans.* **2007**, *9*, 955–964.
[15] J. Lacour, C. Ginglinger, F. Favarger, S. Torche-Haldimann, *Chem. Commun.* **1997**, *23*, 2285–2286.
[16] J.-H. Kim, S.-Y. Kim, S. Choi, H.-J. Son, S. O. Kang, *Inorg. Chem.* **2021**, *60*, 246–262.
[17] Y. Im, S. Y. Byun, J. H. Kim, D. R. Lee, C. S. Oh, K. S. Yook, J. Y. Lee, *Adv. Funct. Mater.* **2017**, *27*, 1603007.
[18] J. H. Lee, C. H. Chen, P. H. Lee, H. Y. Lin, M. K. Leung, T. L. Chiu, C. F. Lin, *J. Mater. Chem. C.* **2019**, *7*, 5874–5888.
[19] O. V. Dolomanov, L. J. Bourhis, R. J. Gildea, J. A. K. Howard, H. Puschmann, *J. Appl. Cryst.* **2009**, *42*, 339–341.
[20] C. F. Macrae, I. Sovago, S. J. Cottrell, P. T. A. Galek, P. McCabe, E. Pidcock, M. Platings, G. P. Shields, J. S. Stevens, M. Towler, P. A. Wood, *J. Appl. Cryst.* **2020**, ***53***, 226–235.
[21] a) G. te Velde, F. M. Bickelhaupt, E. J. Baerends, C. Fonseca Guerra, S. J. A. van Gisbergen, J. G. Snijders, T. Ziegler, *J. Comp. Chem.* **2001**, *22*, 931–967; b) C. Fonseca Guerra, J. G. Snijders, G. te Velde, E. J. Baerends, *Theor. Chem. Acc.* **1998**, *99*, 391–403; c) E. J. Baerends, T. Ziegler, J. Autschbach, D. Bashford, A. Bérces, F. M. Bickelhaupt, C. Bo, P. M. Boerrigter, L. Cavallo, D. P. Chong, L. Deng, R. M. Dickson, D. E. Ellis, M. van Faassen, L. Fan, T. H. Fischer, C. Fonseca Guerra, M. Franchini, A. Ghysels, A. Giammona, S. J. A. van Gisbergen, A. W. Götz, J. A. Groeneveld, O. V. Gritsenko, M. Grüning, S. Gusarov, F. E. Harris, P. van den Hoek, C. R. Jacob, H. Jacobsen, L. Jensen, J. W. Kaminski, G. van Kessel, F. Kootstra, A. Kovalenko, M. V. Krykunov, E. van Lenthe, D. A. McCormack, A. Michalak, M. Mitoraj, S. M. Morton, J. Neugebauer, V. P. Nicu, L. Noodleman, V. P. Osinga, S. Patchkovskii, M. Pavanello, P. H. T. Philipsen, D. Post, C. C. Pye, W. Ravenek, J. I. Rodríguez, P. Ros, P. R. T. Schipper, H. van Schoot, G. Schreckenbach, J. S. Seldenthuis, M. Seth, J. G. Snijders, M. Solà, M. Swart, D. Swerhone, G. te Velde, P. Vernooijs, L. Versluis, L. Visscher, O. Visser, F. Wang, T. A. Wesolowski, E. M. van Wezenbeek, G. Wiesenekker, S. K. Wolff, T. K. Woo, A. L. Yakovlev, ADF2024.1, SCM, Theoretical Chemistry, Vrije Universiteit, Amsterdam, The Netherlands, http://www.scm.com.
[22] C. Adamo, G. E. Scuseria, V. Barone, *J. Chem. Phys.* **1999**, *111*, 2889–2899.
[23] D. P. Chong, *Mol. Phys.* **2005**, *103*, 749–761.
[24] a) A. Klamt, G. J. Schürmann, *J. Chem. Soc. Perkin Trans.* **1993**, *2*, 799–805; b) A. Klamt, V. Jonas, *J. Chem. Phys.* **1996**, *105*, 9972–9981; c) C. C. Pye, T. Ziegler, *Theor. Chem. Acc.* **1999**, *101*, 396–408.

Manuscript received: April 27, 2024
Revised manuscript received: June 11, 2024
Accepted manuscript online: June 17, 2024
Version of record online: September 18, 2024